Mathematical modelling, numerical simulations and experimental verification of bifurcation dynamics of a pendulum driven by a dc motor

2015 Eur. J. Phys. 36 055028

(http://iopscience.iop.org/0143-0807/36/5/055028)

IOP Publishing European Journal of Physics
Eur. J. Phys. **36** (2015) 055028 (13pp) doi:10.1088/0143-0807/36/5/055028

Mathematical modelling, numerical simulations and experimental verification of bifurcation dynamics of a pendulum driven by a dc motor

Marek Kaźmierczak, Grzegorz Kudra, Jan Awrejcewicz and Grzegorz Wasilewski

Lodz University of Technology, Department of Automation, Biomechanics and Mechatronics, 1/15 Stefanowski St. 90-924 Lodz, Poland

E-mail: grzegorz.kudra@p.lodz.pl

Received 7 January 2015, revised 3 April 2015
Accepted for publication 26 May 2015
Published 4 August 2015

Abstract

A mathematical model of a system consisting of a dc motor, mechanism converting the rotational motion to the linear one and a single physical pendulum with the joint horizontally driven is developed. Constant angular velocity of the crank is assumed. The parameters of the model are estimated using the experimental data consisting of five solutions corresponding to the five different values of constant input voltage. Different versions of the mathematical model, with different details concerning friction and damping modelling, are tested. A good agreement between real and simulated behaviour of the system is obtained. Moreover the model is validated by testing its ability to predict critical values of the bifurcation parameter.

Keywords: pendulum, mathematical modelling, dry friction modelling, parameter estimation, bifurcation dynamics

(Some figures may appear in colour only in the online journal)

1. Introduction

A single pendulum and multi-degree systems of pendulums are still subjects of interest to scientists from all over the world and from different areas of science. For mechanics and physicians the pendulum is interesting because of its simultaneous simplicity and

capability of exhibiting many spectacular and fundamental phenomena of bifurcational dynamics.

A large and comprehensive study concerning the pendulum, including a historical review, is presented in [1]. While it easy to find works where single and double pendulums are investigated experimentally [2], much more seldom are experiments performed on systems of more than two pendulums [3, 4]. The plane triple physical pendulum with periodic external forcing acting on the first body was investigated numerically and experimentally in [4], where different versions of models of resistance in the joints, including the viscous damping and dry friction, were tested.

In [5, 6], the plane and periodically forced triple pendulum with rigid limiters of motion was investigated numerically, including stability analysis of the trajectories undergoing discontinuities. In [7], a special case of triple pendulum with barriers, the piston–connecting rod–crankshaft system was presented and investigated.

In [8] the authors investigated numerically a mathematical model of a two-degree-of-freedom electro-mechanical system consisting of a pendulum with support point moving horizontally and driven by the use of two-bar linkage and a dc motor considered as a limited power source. Almost the same system, but investigated both numerically and experimentally, is presented in [13]. In the second case however no chaotic oscillations were observed since the energy dissipation in the system was too high.

For more information on the related problems of nonlinear dynamical systems, deterministic chaos, and bifurcation dynamics, see [9–11], in which the corresponding concepts are presented in a manner appropriate for undergraduate students. The concepts related to modelling of real processes along with the corresponding method of identification and parameter estimation are presented in an accessible way in [12].

The present paper is a modification of the work published in [13], where a more advanced model of the same experimental rig was presented as the initial stage of a larger project and preparation for analysis of the system with periodically varying input voltage of the dc motor. In comparison to the previous work, the experimental rig is developed and equipped with an additional system of measurement of the angular position of the output shaft of the gear box, giving more information for the identification process. On the other hand, the mathematical model is simplified and the angular velocity of the crank is assumed to switch suddenly from zero to a certain constant value, which occurs sufficient for description of the system with similar input voltage behaviour. Results of the paper concern the problems presented and investigated during the laboratory classes within the courses ‘Modelling and Identification of Dynamical System’ and ‘Experimental Method of Mechanics’ at Technical University of Lodz.

The paper is organized as follows. In section 2 there is presented experimental rig, while section 3 presents a mathematical model of the pendulum. In section 4 there are presented results of experimental investigations, parameter estimation and numerical simulations of the presented system. Section 5 presents final remarks and discussion.

2. Experimental rig

Figure 1 exhibits the experimental setup [13], whose mathematical model will be presented in the text part of the paper. A voltage generator 14 supplies the dc motor 1 equipped with the gear transmission 2. On the output shaft of the gearbox there is mounted a disk 3, which rotational motion is transformed, using the link 4-5-6, to the linear motion of the slider 7-8 moving along the horizontal guide 12-13. On the slider there is suspended physical pendulum

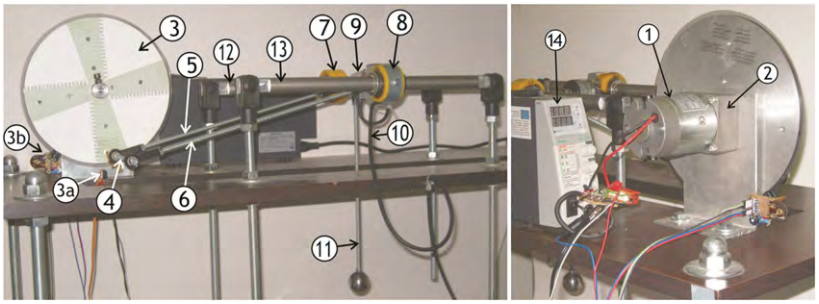

Figure 1. Experimental setup.

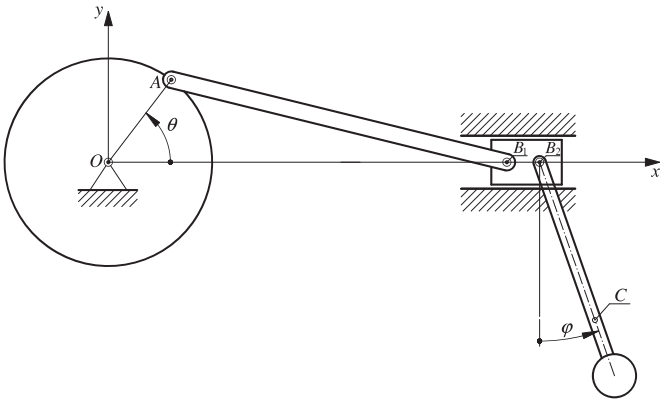

Figure 2. Mechanical system.

11, whose angular position is measured by the use of potentiometer 9 supplied by wire 10. The angular position of disk 1 is measured by the use of an angular scale situated on its circumference and incremental angle transducer equipped with the optocoupler sensor 3b. For additional control of correct operation of the measurement system, the experimental rig is equipped with optocoupler sensor 3a detecting the angular position of the disk $\theta = -\pi/2$ (see section 3).

3. Physical and mathematical modelling

Physical conception of the system is presented in figure 2 [13]. It is a plane system consisting of four rigid bodies: disk (crank OA) of angular position described by the angle $\theta(t)$ being a predetermined function of time, connecting rod AB_1, horizontally moving the slider and pendulum of angular position described by the angle $\varphi(t)$. It is assumed, according to the structure of the experimental rig, that the pendulum is connected to the slider by the use of the rotational joint B_2. Under the above-mentioned assumptions the system possess one degree of freedom, since its position is defined uniquely by the angle $\varphi(t)$.

The governing differential equations will be derived by the use of the Lagrange equations of the second kind, which for the analyzed system take the following form

$$\frac{\mathrm{d}}{\mathrm{d}t}\left(\frac{\partial T}{\partial \dot{\varphi}}\right) - \frac{\partial T}{\partial \varphi} + \frac{\partial V}{\partial \varphi} = Q, \tag{1}$$

where T and V are kinetic and potential energies, while φ and Q are the generalized coordinate and the corresponding generalized force acting on the system.

The kinetic energy reads

$$T = \frac{1}{2}m\left(\dot{x}_C^2 + \dot{y}_C^2\right) + \frac{1}{2}I\dot{\varphi}^2, \tag{2}$$

where m is mass of the pendulum and I is its moment of inertia with respect to the axis perpendicular to the motion plane and including the pendulum's mass centre C, whose position is defined by the two coordinates x_C and y_C in the coordinate system Oxy shown in figure 2. They can be expressed in the following way

$$\begin{aligned} x_C(t) &= s(t) + r\sin\varphi(t), \\ y_C(t) &= -r\cos\varphi(t), \end{aligned} \tag{3}$$

where $s(t) = xB_2(t)$ is horizontal position of the point B_2 and r is length B_2C defining position of the point C.

Taking into account equation (3), the kinetic energy (2) takes the following form

$$T = \frac{1}{2}m\,\dot{s}^2 + m\,r\,\dot{s}\,\dot{\varphi}\cos\varphi \; + \frac{1}{2}B\dot{\varphi}^2, \tag{4}$$

where the following notation is introduced

$$B = I + m\,r^2.$$

The potential energy is related to the potential of the gravitational force acting on the pendulum and horizontal position of the point C

$$V = -m\,g\,r\,\cos\,\varphi, \tag{5}$$

where g is the gravitational constant.

The generalized force Q represents the remaining and non-potential forces acting on the system. It will be used to model resistance torque acting on the pendulum in the joint B_2. Let us assume the existence of both dry friction and linear damping in the joint B_2. Then the generalized force Q can be modelled in the following way

$$Q = -c_B\dot{\varphi} - \frac{2}{\pi}M_B\arctan(\varepsilon\dot{\varphi}), \tag{6}$$

where c_B is damping coefficient and M_B is magnitude of dry friction torque $M_B\,\mathrm{sign}(\dot{\varphi})$, where the sign function is approximated by the use of the arctan function and where ε is a relatively large positive parameter.

Taking into account the relations (4)–(6), equation (1) takes the form

$$B\ddot{\varphi} + c_B\dot{\varphi} + \frac{2}{\pi}M_B\arctan(\varepsilon\dot{\varphi}) + S\,g\,\sin\varphi + S\,\ddot{s}\cos\varphi = 0, \tag{7}$$

where

$$S = m\,r.$$

Horizontal position s of the slider can be described as follows

$$s(t) = a\left(\cos\theta(t) + \lambda^{-1}\sqrt{1 - \lambda^2\sin^2\theta(t)}\right), \tag{8}$$

where

$$\lambda = \frac{a}{b}.$$

Then the second derivative of s, which appears in the governing equation (7), has the following form

$$\ddot{s} = -a\left(\cos\theta + G\cos 2\theta + \frac{1}{4}G^3\sin^2 2\theta\right)\dot{\theta}^2 - a\sin\theta(1 + G\cos\theta)\ddot{\theta}, \tag{9}$$

where

$$G = \frac{\lambda}{\sqrt{1 - \lambda^2\sin^2\theta(t)}}. \tag{10}$$

Using the relation (9) in equation (7), one obtains the following final form of the governing equation

$$\ddot{\varphi} + c'_B\,\dot{\varphi} + \frac{2}{\pi}M'_B\arctan(\varepsilon\dot{\varphi}) + S'\,g\,\sin\varphi + S'\,\ddot{s}\cos\varphi = 0, \tag{11}$$

where

$$c'_B = \frac{c_B}{B},\ M'_B = \frac{M_B}{B},\ S' = \frac{S}{B}.$$

4. Numerical versus experimental investigations

4.1. Parameter estimation

In this section $\xi_e(t)$ denotes experimental counterpart of the signal $\xi(t)$ occurring in the mathematical model of the system. In the identification process we use five sets of experimental signals $\varphi_e(t)$ and $\theta_e(t)$ corresponding to different values of almost constant input voltage (stabilized by the voltage generator) of the dc motor, recorded on the time interval [0, 60] s. Values and derivatives with respect to time of the measured signals at the initial instance $t=0$ are known and the same for all five cases: $\varphi_e(0)$ 0 rad, $\dot{\varphi}_e(0) = 0\,\frac{\text{rad}}{\text{s}}$, $\theta_e(0) = -\frac{\pi}{2}$rad and $\dot{\theta}_e(0) = 0\,\frac{\text{rad}}{\text{s}}$.

Figure 3 exhibits behaviour of the functions $\Delta\theta_e(t) = \theta_e(t) - \theta_{eL}(t)$, where $\theta_{eL}(t) = b_0 + \omega_e t$ is a linear approximation of the angle $\theta_e(t)$ for $t \in [0,\ 60]s$, for each experimental solution. One can conclude that because of the non-ideal behaviour of resistances in the system (small random fluctuations of friction), the angular velocity of the disk undergoes some random changes, which cannot be described by the use of deterministic equations. These changes are not big, but after some time they can lead to a significant time shift in the angular position of the disk. It may cause problems in fitting the simulated signals to those obtained experimentally, if we express them in the time domain. This is the reason why we compare the corresponding signals expressed as functions of angular position of the disk.

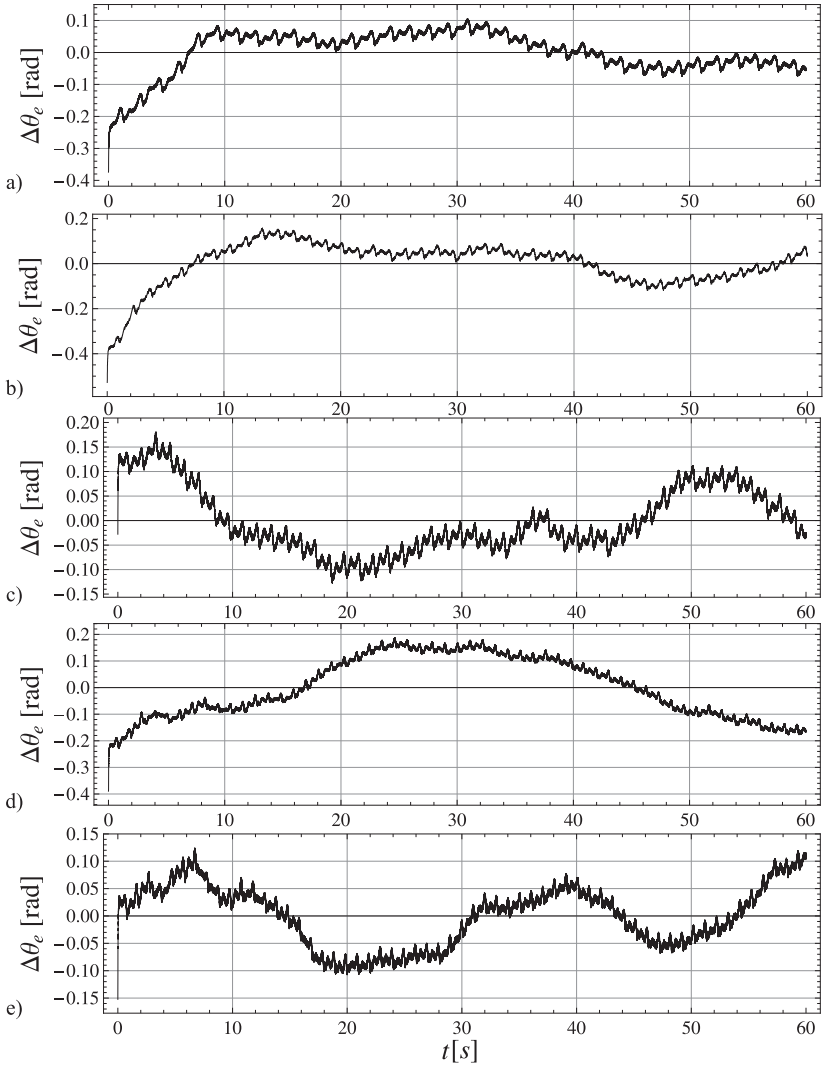

Figure 3. The behaviour of the functions $\Delta\theta_e(t) = \theta_e(t) - \theta_{eL}(t)$, where $\theta_{eL}(t)$ is a linear function approximating the experimental angle $\theta_e(t)$ for $t \in [0,\ 60]s$, for five experimental solutions ($u_e = -5.063$, -6.049, -6.518, -7.503 and -8.024 V, for (a)–(e), respectively).

Table 1. Average input voltages and angular velocities of the dc motor.

Number i of the experimental solution	1	2	3	4	5
Average experimental voltage u_{ei} [V]	−5.063	−6.049	−6.518	−7.503	−8.024
Average experimental angular velocity ω_{ei} [rad/s]	−3.797	−4.591	−4.961	−5.796	−6.215

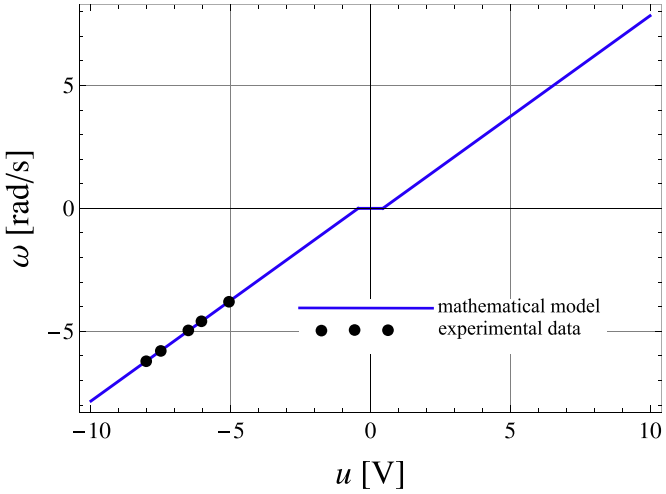

Figure 4. The relation between angular velocity ω of the crank and input voltage u of the dc motor: mathematical model (11) (blue line) and experimental data (black dots).

Table 1 exhibits average input voltage u_e and average angular velocity ω_e of the crank for each experimental solution. This data can be approximated by the following piece-wise linear relation

$$\omega = \begin{cases} a_0 + a_1 u & \text{for } u < -a_0/a_1 \\ 0 & \text{for } u \in \left[-a_0/a_1,\, a_0/a_1\right] \\ -a_0 + a_1 u & \text{for } u > a_0/a_1 \end{cases} \tag{12}$$

where $a_0 = 0.3618$ rad/s and $a_1 = 0.8194$ (rad/s)/V. Figure 4 presents the relation (12) along with the corresponding experimental data.

Fitting the model (11) to the experimental data, the same initial state of the model and real system are assumed. However in the case of the model we assume at the initial instance a jump of angular velocity $\dot{\theta}(t)$ of the crank from zero to the constant value ω. This jump can be interpreted as an impact and is related to the simultaneous jump of the velocity $\dot{\varphi}$ of the pendulum. Replacing in equations (11) and (9) the second derivatives with respect to the time by the quotients of small increments of the corresponding variables, one gets

$$\frac{\Delta\dot{\varphi}}{\Delta t} + c_B'\dot{\varphi} + \frac{2}{\pi}M_B' \arctan(\varepsilon\dot{\varphi}) + S'\, g\, \sin\varphi + \\ - S'\, a\left(\left(\cos\theta + G\cos 2\theta + \frac{1}{4}G^3\sin^2 2\theta\right)\dot{\theta}^2 + \sin\theta(1 + G\cos\theta)\frac{\Delta\dot{\theta}}{\Delta t}\right)\cos\varphi = 0. \tag{13}$$

Multiplying the above equation by Δt and dropping off the infinitely small terms (under assumption of infinitely short duration Δt of the impact), one obtains the following relation between the jumps of the velocities of the pendulum $\Delta\dot{\varphi}$ and the crank $\Delta\dot{\theta}$

$$\Delta\dot{\varphi} - S'\, a \sin\theta\cos\varphi(1 + G\cos\theta)\,\Delta\dot{\theta} = 0. \tag{14}$$

Limiting the considerations to the case of the model position equal to the initial position of the experimental system ($\varphi = 0$ and $\theta = -\frac{\pi}{2}$rad), equation (14) simplifies to the following

Table 2. Model parameters obtained in the identification process.

Parameter/Model	**A**	**B**	**C**	**D**	**E**
$10^3 \cdot F_O$ [rad^2]	6.915	4.242	3.676	3.612	3.802
S' [m^{-1}]	3.692	3.632	3.647	3.643	3.634
c'_B [s^{-1}]	0.328	0	0.087	0.047	0
M'_B [s^{-2}]	0	1.719	1.267	1.608	1.834
ε	10^3	10^3	10^3	2.243	2.900

form

$$\Delta\dot{\varphi} = -aS'\,\Delta\dot{\theta}. \tag{15}$$

Then the initial velocity of the pendulum during the proper simulation (after the impact, when $\dot{\theta} = \omega = \text{const}$, $\ddot{\theta} = 0$) reads

$$\dot{\varphi}(0) = -aS'\,\omega. \tag{16}$$

During the parameter estimation, the following construction of the objective function is used

$$F_O(\boldsymbol{\mu}) = \frac{1}{\sum_{i=1}^{N}\left(\theta_{\max i} - \theta_{\min i}\right)} \sum_{i=1}^{N} \int_{\theta_{\min i}}^{\theta_{\max i}} \left(\varphi_i(\theta, \boldsymbol{\mu}) - \varphi_{ei}(\theta)\right)^2 \mathrm{d}\theta, \tag{17}$$

where N denotes number of the compared pairs of solutions, φ_i and φ_{ei} are angular positions of the pendulum obtained by the use of ith numerical simulation and experiment, while $\boldsymbol{\mu}$ is vector of the estimated parameters. It is assumed that $\theta = \theta_e$ and each simulation is performed until the angle θ reaches $\theta_{\min}$. It is also assumed that $\omega = \omega_e$. Function (17) represents the average squared deviation between signals obtained during numerical simulation and the corresponding experimental data. Therefore it allows assessing the quality of the model and its parameters.

Some of the system parameters, which are relatively easy to determine, are assumed as known: $a = 0.090$ m, $\lambda = 0.2535$, $g = 9.81$ m·s^{-2}. The other parameters, as elements of the vector $\boldsymbol{\mu}$, are estimated by minimizing the objective function (17). For the global minimum search the Nelder–Mead method [14], also known as the downhill simplex method, is used. This is a commonly used optimization algorithm, implemented in Matlab and Scilab as the function *fminsearch*. However, one should be careful of stopping the algorithm in a local minimum, which is not the desired solution. In order to avoid such a mistake one should perform the optimization using different starting points (initial guesses of the solution) of the method.

Five different versions of the model are tested: A, where it is assumed that only viscous damping in the joint B_2 (based on the rolling bearings) is present $\left(\boldsymbol{\mu} = \left[S',\ c'_B\right],\ M'_B = 0\right)$; B, assuming only dry friction in the joint B_2 $\left(\boldsymbol{\mu} = \left[S',\ M'_B\right],\ c'_B = 0,\ \varepsilon = 10^3\right)$; C, assuming both the viscous damping and dry friction in the joint B_2 $\left(\boldsymbol{\mu} = \left[S',\ c'_B,\ M'_B\right],\ \varepsilon = 10^3\right)$; D, being a modification of the model C, assuming additionally that the parameter ε is an element of the vector of the estimated parameters $\left(\boldsymbol{\mu} = \left[S',\ c'_B,\ M'_B,\ \varepsilon\right]\right)$; and E, built on the base of the model D, assuming no viscous damping $\left(\boldsymbol{\mu} = \left[S',\ M'_B,\ \varepsilon\right], c'_B = 0\right)$.

Table 2 presents results of the parameter estimation for the tested models. Analyzing the final values of the objective functions, one can conclude that assumption of only the viscous damping (model A) or only dry friction (model B) in the joint B_2 is not sufficient, while assumption of both of them leads (model C) to much better results. According to the initial assumptions, the parameter ε should be relatively large in order to approximate the sign function. It occurs however that smaller values of this parameter may lead to better results (model D). The improvement is rather slight but there is another advantage of model D, i.e. avoiding the stiffness of the differential equations and better performance of the numerical solvers. Removal of the viscous damping term from model D (model E) leads to slightly worse results. Figure 5 exhibits a comparison of five numerical solutions $\varphi(\theta)$ to the best model (D) with the corresponding experimental data $\varphi_e(\theta)$ at the end of the identification process. The same solutions, but plotted on the interval $-\theta \in [200,\ 225]$ rad, are presented in figure 6.

4.2. Further numerical and experimental investigations

Figure 7 presents a bifurcation diagram [9–11] of the mathematical model D, where the constant angular velocity ω plays the role of control parameter. In the construction of this bifurcational diagram the Poincaré map has been used, which is equivalent to the section of the attractor by the plane $\theta = -\frac{\pi}{2}\text{rad}$, with a condition that θ is falling. Changing the control parameter with a small step from its minimal to maximal value, for each value of the control parameter, after ignoring some transient motion, one such Poincaré map is performed. Initial conditions for each solution are equal to the final state of the previous one. Using this method one obtains branch B and a part of curve A. Then the same process is repeated changing the control parameter from its maximal to minimal value, allowing one to find all of branch A and a part of curve B. Branches A and B correspond to two different stable periodic orbits A and B, undergoing two saddle-node bifurcations SNA and SNB. In the saddle-node bifurcation, when the control parameter is changed, two solutions, stable and unstable, meet each other and disappear together. The dashed curve denoting the unstable periodic orbit has only a qualitative character. Between the critical values of the control parameter corresponding to the bifurcations SNA and SNB, there exists a region of the coexistence of two stable periodic solutions A and B. Figure 7 also depicts the solutions used in the identification process.

The critical parameters corresponding to the saddle-node bifurcations are then investigated more carefully for all tested models, as well as experimentally. The results are presented in table 3. During the experimental investigations the input voltage is changed continuously with a speed of 0.03 V/min (then the corresponding angular velocity ω is computed using the function (12)). Numerical analysis is done by changing the control parameter ω with a step of 0.0005 rad/s. Magnitude of the corresponding parameter is increased in order to detect the SNA bifurcation, while it is increased in order to detect the SNB bifurcation. In all cases a jump of the solution indicates the saddle-node bifurcation and limit of existence of the stable attractor.

5. Concluding remarks and discussion

In the paper the simplified version of the model of the pendulum driven by a dc motor, being a part of a larger project, was presented. In particular, the angular velocity of the crank was

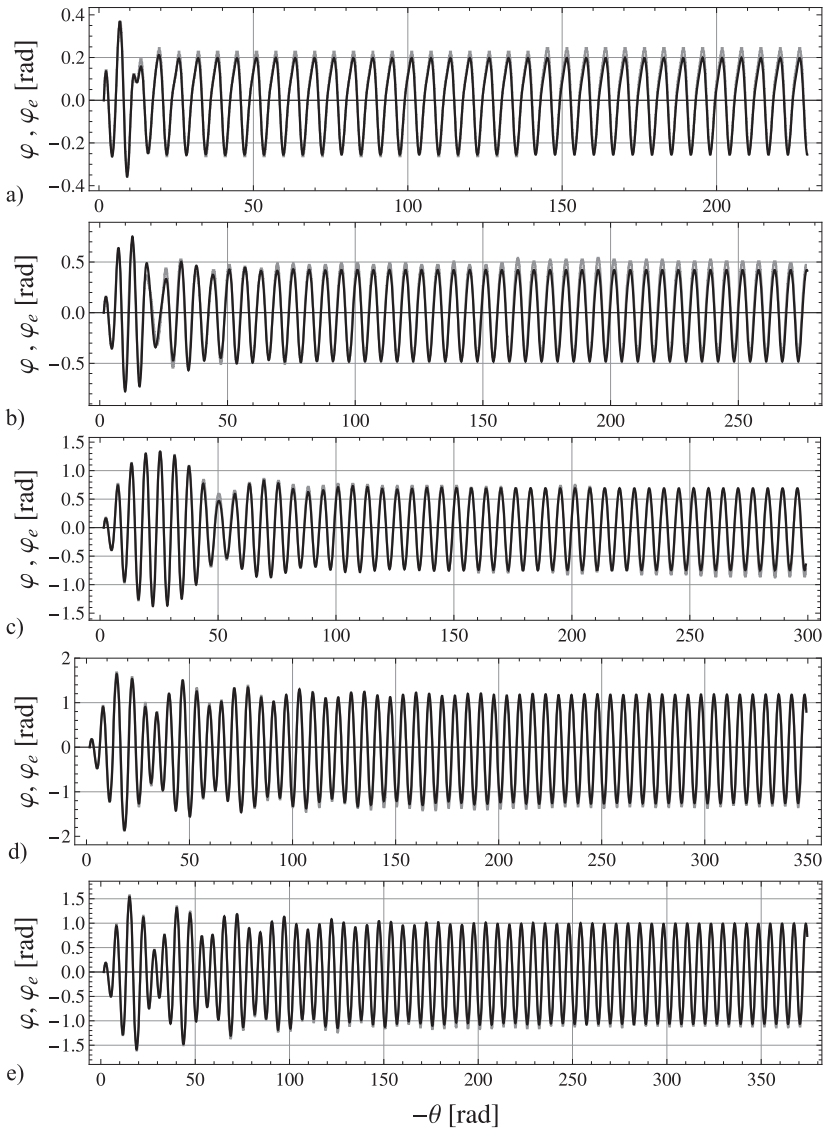

Figure 5. Five numerical solutions $\varphi(\theta)$ to the model D (black line), compared with the experimental data $\varphi_e(\theta_e)$ (gray line), at the end of the identification process (u_e = −5.063, −6.049, −6.518, −7.503 and −8.024 V, for (a)–(e), respectively).

assumed as a predetermined function of time, reducing the number of degrees of freedom to one. The aim of the paper was to present as simple as possible an approach in modelling, analysis and prediction of bifurcation dynamics of a simple real system.

Different versions of the model of resistance in the pendulum joint based on the rolling bearings were tested. One can conclude that taking into account only viscous damping or only dry friction in the joint is not sufficient. Assumption of both of them leads to significantly better results. Moreover a modification of the approximation of the sign function in the

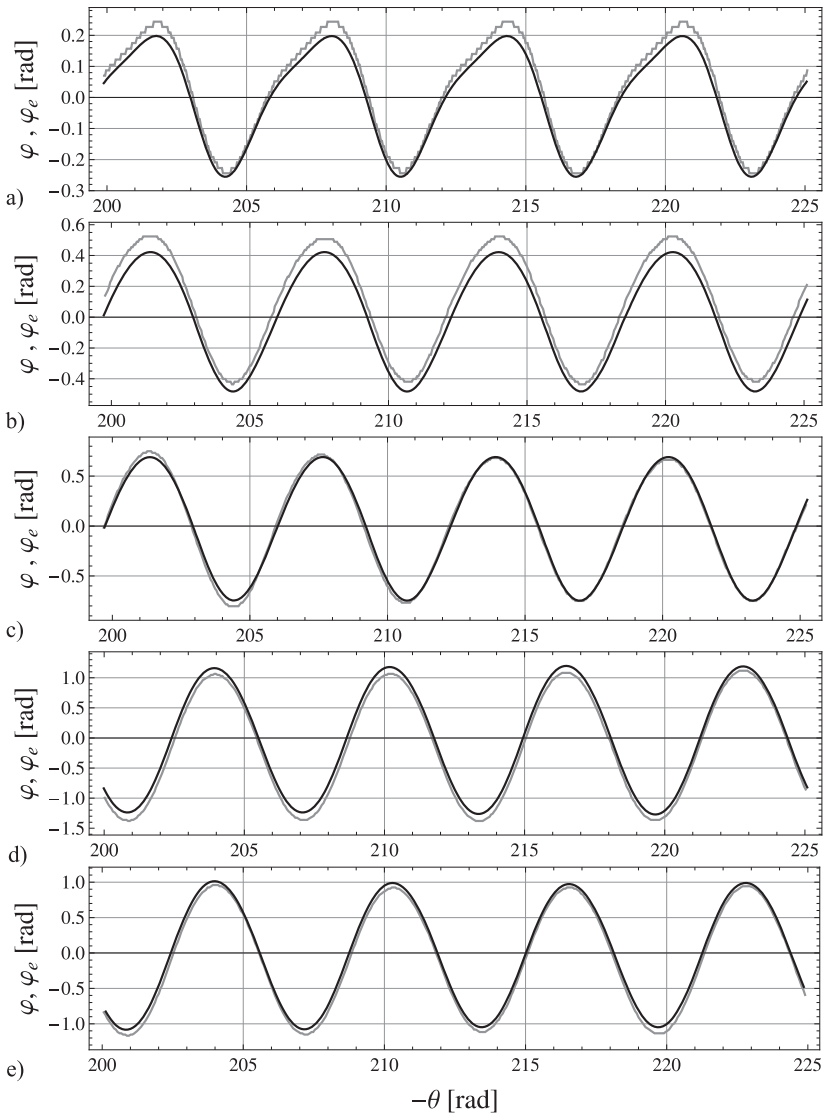

Figure 6. Five numerical solutions $\varphi(\theta)$ to the model D (black line), compared on the interval $-\theta \in [200,\ 225]$rad with the experimental data (gray line), at the end of the identification process ($u_e = -5.063$, -6.049, -6.518, -7.503 and -8.024 V, for (a)–(e), respectively).

description of the dry friction were performed, leading to another kind of nonlinear resistance, giving slightly better results and avoiding stiffness of the governing differential equations.

The developed model yielded a good tool for analysis, explanation and prediction of nonlinear dynamics of the presented real pendulum. In particular, the critical values of the control parameter corresponding to the saddle-node bifurcations were predicted numerically and then confirmed experimentally.

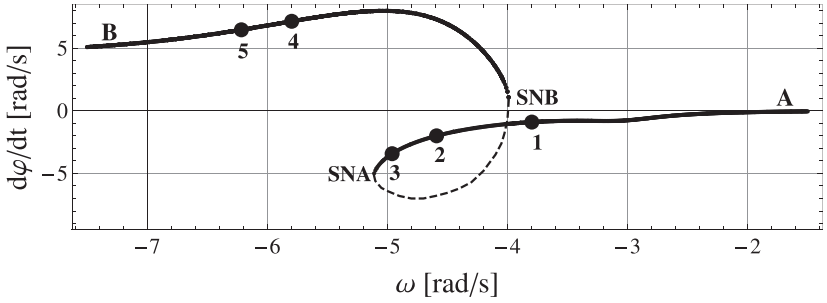

Figure 7. Bifurcation diagram of the mathematical model exhibiting a region of coexistence of two periodic attractors A and B, with five marked points corresponding to the solutions exhibited by figures 5 and 6.

Table 3. Critical parameters corresponding to the saddle-node bifurcations detected experimentally and numerically.

	Experiment	A	B	C	D	E
$\omega_{SNA}\left[\frac{\text{rad}}{\text{s}}\right]$	−5.160	−5.146	−5.111	−5.120	−5.119	−5.113
$\omega_{SNB}\left[\frac{\text{rad}}{\text{s}}\right]$	−4.038	−4.300	−3.879	−4.013	−3.985	−3.907

Acknowledgements

This work has been supported by the Polish National Science Centre, MAESTRO 2, No. 2012/04/A/ST8/00738.

References

[1] Baker G L and Blackburn J A 2005 *The Pendulum. A Case Study in Physics* (Oxford: Oxford University Press)
[2] Blackburn J A, Zhou-Jing Y, Vik S, Smith H J T and Nerenberg M A H 1987 Experimental study of chaos in a driven pendulum *Physica* D **26** 385–95
[3] Zhu Q and Ishitobi M 1999 Experimental study of chaos in a driven triple pendulum *J. Sound Vib.* **227** 230–8
[4] Awrejcewicz J, Supeł B, Kudra G, Wasilewski G and Olejnik P 2008 Numerical and experimental study of regular and chaotic motion of triple physical pendulum *Int. J. Bifurcation Chaos* **18** 2883–915
[5] Awrejcewicz J, Kudra G and Lamarque C-H 2003 Dynamics investigation of three coupled rods with a horizontal barrier *Meccanica* **38** 687–98
[6] Awrejcewicz J, Kudra G and Lamarque C-H 2004 Investigation of triple physical pendulum using fundamental solution matrices *Int. J. Bifurcation Chaos* **14** 4191–213
[7] Awrejcewicz J and Kudra G 2005 The piston–connecting rod–crankshaft system as a triple physical pendulum with impacts *Int. J. Bifurcation Chaos* **15** 2207–26
[8] Belato D, Weber H I, Balthazar J M and Mook D T 2001 Chaotic vibrations of a nonideal electro-mechanical system *Int. J. Solids Struct.* **38** 1699–706
[9] Kaplan D 1997 *Understanding Nonlinear Dynamics* (Berlin: Springer)
[10] Wiggins S 2003 *Introduction to Applied Nonlinear Dynamical Systems and Chaos* (Berlin: Springer)
[11] Strogatz S H 2001 *Nonlinear Dynamics and Chaos with Applications to Physics, Biology, Chemistry, and Engineering* (Jackson, TN: Perseus Books Publishing)

[12] Gershenfeld N 2011 *The Nature of Mathematical Modelling* (Cambridge: Cambridge University Press)
[13] Kaźmierczak M, Kudra G, Awrejcewicz J and Wasilewski G 2013 Numerical and experimental investigation of bifurcational dynamics of an electromechanical system consisting of a physical pendulum and dc motor *Dynamical Systems—Applications* ed J Awrejcewicz, M Kaźmierczak, P Olejnik and J Mrozowski J (Lodz: TU of Lodz Press) pp 49–58
[14] Nelder J A and Mead R 1965 A simplex method for function minimization *Comput. J.* **7** 308–13